EFDA–JET–PR(11)43

D. Stoyanov, M.N.A. Beurskens, T. Dreischuh, L. Gurdev, O. Ford, J. Flanagan,
M. Kempenaars, I. Balboa, M. Walsh and JET EFDA contributors

Deconvolution-Based Retrieving of Plasma Electron Temperature Pedestal from Thomson Scattering JET Core LIDAR Data

Deconvolution-Based Retrieving of Plasma Electron Temperature Pedestal from Thomson Scattering JET Core LIDAR Data

D. Stoyanov[1], M.N.A. Beurskens[2], T. Dreischuh[1], L. Gurdev[1], O. Ford[2], J. Flanagan[2], M. Kempenaars[2], I. Balboa[2], M. Walsh[2] and JET EFDA contributors*

JET-EFDA, Culham Science Centre, OX14 3DB, Abingdon, UK

[1]Institute of Electronics, Bulgarian Academy of Sciences and EURATOM/INRNE Fusion Association, 72 Tzarigradsko Shosse, Sofia, Bulgaria
[2]EURATOM-CCFE Fusion Association, Culham Science Centre, OX14 3DB, Abingdon, OXON, UK
** See annex of F. Romanelli et al, "Overview of JET Results", (23rd IAEA Fusion Energy Conference, Daejon, Republic of Korea (2010)).*

Preprint of Paper to be submitted for publication in
Review of Scientific Instruments

“This document is intended for publication in the open literature. It is made available on the understanding that it may not be further circulated and extracts or references may not be published prior to publication of the original when applicable, or without the consent of the Publications Officer, EFDA, Culham Science Centre, Abingdon, Oxon, OX14 3DB, UK.”

“Enquiries about Copyright and reproduction should be addressed to the Publications Officer, EFDA, Culham Science Centre, Abingdon, Oxon, OX14 3DB, UK.”

The contents of this preprint and all other JET EFDA Preprints and Conference Papers are available to view online free at www.iop.org/Jet. This site has full search facilities and e-mail alert options. The diagrams contained within the PDFs on this site are hyperlinked from the year 1996 onwards.

ABSTRACT.
We demonstrate the resolving of the electron temperature pedestal from the Thomson scattering Core LIDAR data in the JET tokamak. The proposed novel method is based on the deconvolution of Core LIDAR profiles and the use of a specific fitting algorithm applied to the deconvolved and convolved (by a defined low-pass filter) estimates of electron temperature profiles of variable pedestal parameters. We present this method in preparation of the expected upgrade of the core LIDAR system in terms detector sensitivity and higher sampling rate of the digitisers. The method application to the current JET Core LIDAR data requires over-sampling of original LIDAR profiles (3 cm step) to a new sampling scale of 1 cm step. Then we apply an optimal three-parameter least-square algorithm to extract the best fit of the electron temperature pedestal parameters (amplitude, width and position) at a given pedestal shape. As a result, we retrieve the electron temperature profile over the entire plasma diameter with a step of 1cm, including the resolved pedestal. The simulation analysis by a computer model, based on the TS Core LIDAR parameters, demonstrates the expected performance of the full processing algorithm based on the novel method.

1. INTRODUCTION

The high-confinement mode (H-mode) is one of the most promising regimes of operation of the thermonuclear fusion experiments such as the Joint European Torus (JET), characterized by the formation of a narrow edge pedestal area, where steep gradients in the electron density and temperature are observed as a result of formation of a particle and energy transport barrier near the plasma edge. So, the possibility of determining the plasma pedestal characteristics in the pedestal area with a high resolution is of great importance for the better understanding of processes on the plasma edge.

A number of diagnostic instruments based on different operation principles are used in JET for determination of plasma electron temperature T_e and density n_e profiles inside the torus. The Thomson Scattering (TS) [1-3] has been successfully used for reliable and robust simultaneous measurement of T_e and n_e profiles on JET. The TS Core LIDAR system is one of the default diagnostics on JET. The High Resolution Thomson Scattering (HRTS) system [4,5] is another powerful instrument for determination of T_e and n_e profiles with a high resolution ($\leq$1cm), providing a valuable information about the plasma edge. The other diagnostic instruments such as the Edge LIDAR [3], the Electron – Cyclotron Emission (ECE) radiometer and the Michelson Interferometer are also of great importance for the analysis of the plasma temporal and spatial behavior. The joint use of different diagnostic instruments is generally accepted as the best approach for reliable data interpretation of the thermonuclear plasma behavior.

One of the basic advantages of the TS Core LIDAR (figure 1) is the opportunity to measure T_e and n_e profiles simultaneously along the entire plasma diameter. The LIDAR resolution is however of the order of 12cm and thus it is practically insufficient for resolving the narrow edge pedestal area, which has a typical length scale in the range of 2cm to 5cm. Therefore, the enhancement

of Core LIDAR resolution is considered as an important task for improving the JET plasma diagnostics as a whole. The hardware upgrade with modern detectors and data acquisitions blocks is one of the promising approaches toward the resolving of plasma pedestals. For example, it has been estimated that improvements of both the spatial resolution and the Signal-to-Noise Ratio (SNR) can be obtained by replacing the existing detectors with faster and more sensitive GaAsP detectors [3,6]. It was also shown that in addition the upgrading of the existing digitizer from a 1 GHz bandwidth device with 5 GSa/s to a digitizer with a 4GHz bandwidth with 20 GSa/s will reduce the overall system resolution to a 7 cm at a three-fold improvement of the SNR [3].

Deconvolution is a powerful approach [7-11] for software improving the resolution of LIDAR systems. In our case, an enhancement of the Core LIDAR resolving power can also be obtained by applying a deconvolution to each of the LIDAR signals from the six TS spectral channels using the system instrument function, as has been demonstrated in [12,13]. The resultant deconvolution improvement of the resolution is about 3 times, but is still insufficient to restore accurately the pedestal area. The restored temperature and density profiles (retrieved from the deconvolved LIDAR profiles) still remain seemingly extended outside the torus wall.

In this paper we are doing the next step toward the estimation of the true shape of the electron temperature pedestal from the Core LIDAR data. The basic goal is to apply a novel deconvolution-based method we have developed to the present data of 3 cm sampling step. It is of essential importance for estimation of the performance of the method and evaluation of its advantages and limitations. The method will be used also after the expected upgrading of the LIDAR receiving & acquisition system with novel detectors and digitizers. It is compatible with the future ITER TS LIDAR data as well.

The optimal performance of the method and the corresponding algorithms requires data sampling steps ≤1cm. To this end, we have used an original approach [14,15] to transforming the present input LIDAR profiles (3cm step) to a finer range step of 1cm. The performance of the novel method was tested by simulations and by processing real data for plasmas of high triangularity. The simulation analysis by a computer model based on Core LIDAR parameters demonstrates the expected performance of the full processing chain. The resolving of the electron temperature pedestal using Core LIDAR TS data (demonstrated for the first time in this work) contributes to the increasing of the information quality of plasma diagnostics.

2. FEATURES OF THE DECONVOLUTION FOR RETRIEVING THE TRUE ELECTRON TEMPERATURE PEDESTAL FROM JET TS CORE LIDAR DATA

As an inverse procedure the deconvolution is noise sensitive. The noises impose limitations on the achievable resolution after the deconvolution. To estimate their effect, let us consider the LIDAR profiles L_p along a Line Of Sight (LOS) coordinate r in the *p-th* spectral channel, $p = 1..6$. The registered (convolved) LIDAR profile L_p^{con} (after passing through the entire set of Core LIDAR blocks) is given by the convolution:

$$L_p^{con}(r) = L_p^{true}(r) \otimes R_{lid}(r) + V_p^{con}(r), \tag{1}$$

where L_p^{true} is the true LIDAR profile, corresponding to δ-type laser pulse shape and instrument functions of the detection and digitizing systems; $R_{lid}(r)=R_{las}(r)\otimes R_{det}(r)\otimes R_{adc}(r)$ is the normalized total LIDAR instrument function, expressed by the partial instrument functions of its basic subsystem blocks: $R_{las}(r)$ is the laser pulse shape, $R_{det}(r)$ is the detector instrument function, and $R_{adc}(r)$ is the instrument function of the analog-to-digital converter (ADC); V_p^{con} are the convolved (correlated) output noses due to the Poisson fluctuations of the signal and background (plasma light) number of photons, to sampling noises, etc.; ⊗ denotes convolution. To restore the LIDAR profiles that would be registered with a short instrument function, the deconvolution approach could be used. The deconvolution is expressed by the inverse transformation:

$$L_p^{dcv}(r) = L_p^{con}(r) \otimes^{-1} R_{lid}(r) + V_p^{dcv}(r), \tag{2}$$

where $L_p^{true}(r)$ are the deconvolved LIDAR profiles, $V_p^{dcv}(r)$ are deconvolved noises, and $\otimes^{-1}$ denotes deconvolution. The Fourier spectra of the convolved LIDAR profiles $L_p^{con}(\omega)$ are:

$$L_p^{con}(\omega) = L_p^{true}(\omega)\, R_{lid}(\omega) + V_p^{con}(\omega), \tag{3}$$

where $L_p^{true}(\omega)$ are the Fourier spectra of the true LIDAR profiles, $V_p^{con}(\omega)$ are the noise spectra in convolved profiles and $R_{lid}(\omega)$ is the spectrum of the total instrument function. The spectra of deconvolved profiles are expressed now by

$$L_p^{dcv}(\omega) = L_p^{con}(\omega) \big/ R_{lid}(\omega) = L_p^{true}(\omega) + V_p^{con}(\omega) \big/ R(\omega). \tag{4}$$

In (4) we assumed the condition $R_{lid}(\omega) \neq 0$ to be fulfilled within the entire Nyquist interval $-\omega_N \leq \omega \leq \omega_N$; $\omega_N = \pi/\Delta t$ is the Nyquist frequency and Δt is the temporal sampling step of the acquisition system. In spite of this condition, the spectrum of $R_{lid}(\omega)$ tends as a rule to low spectral levels at higher frequencies $\omega \rightarrow \omega_N$, while the noise spectrum of convolved signals remains relatively constant or $V_p^{con}(\omega \rightarrow \omega_N) \approx \text{const} >> R_{lid}(\omega \rightarrow \omega_N)$. This results in unacceptable high noise levels in the second term on the right-hand side of (4) with respect to the deconvolved LIDAR profiles (the first term in (4)). The restriction of the high frequency noise influence on the deconvolved signals can be realized by using some Low-Pass Filters (LPF) of proper characteristics $H(\omega)$:

$$L_p^{dcv}(\omega) H(\omega) = L_p^{true}(\omega) H(\omega) + V_p^{con}(\omega) H(\omega) \big/ R(\omega). \tag{5}$$

The last expression can also be presented in the integral form :

$$L_p^{dcv}(r) = L_p^{true}(r) \otimes H(r) + V_p^{dcv}(r) \tag{6}$$

where $H(r)$ is the LPF characteristics in the range domain; $V_p^{dcv}(r)$ are filtered deconvolved noises in the range domain. Thus, although deconvolved, the output LIDAR profiles in (6) remain residually convolved by the LPF characteristic $H(r)$. This convolution can not be practically avoided in the case of JET pedestals, because of their wide spectra covering the entire Nyquist interval.

The problem is illustrated in figure 2 where the modeled electron temperature profiles are presented. The input parameters accepted in the model are close to those of the JET Core LIDAR system. As seen, the electron temperature profiles $T_e^{con}(r)$ and $T_e^{dcv}(r)$ retrieved from the convolved and deconvolved LIDAR profiles, respectively, are extended outside the torus wall because of the convolution of true LIDAR profiles with the instrument function and with the LPF characteristic. The deconvolution leads to closer disposition of the end of $T_e^{dcv}(r)$ to the wall as well as to its steeper tending to zero. The requirements to the low pass filter $H(r)$ could be reduced by upgrading the LIDAR hardware as noted above, but still not fully eliminates the need of $H(r)$.

Resuming, if using only a deconvolution one can not fully retrieve the true electron temperature and density pedestals from Core LIDAR data. Therefore, we have to look for some additional approaches to their determination. The deconvolution can be considered as an intermediate, but necessary step toward the true pedestal estimation from the JET Core LIDAR data. We should note here the very important fact that the LPF characteristic $H(r)$ is a well known, preliminary chosen function. Below we will show that $T_e^{con}(r)$ and $T_e^{dcv}(r)$ profiles together with the well defined function $H(r)$ can be used for the development of a novel method for estimation of the true electron temperature pedestal from the JET Core LIDAR data.

3. GENERAL BLOCK-SCHEMATIC

The general block-schematic of the processing chain is presented in figure 3. The input data are the standard JET Core LIDAR data, containing sets of LIDAR profiles in six spectral channels per each laser shot (~ 140 shots per plasma pulse). The input LIDAR data enter the block 1 for a transformation of LIDAR profiles to a new, finer sampling step. Then, the convolved and deconvolved electron temperature in the new sampling step are retrieved and further used by the optimal algorithm in the block 2 for retrieving the estimates of the true pedestal in the finer sampling step.

In order to obtain some description of the pedestal area we need to have more detailed sampled LIDAR data compared to the present LIDAR data recorded with a sampling step $\Delta r = c\Delta t/2 =$ 3cm; c is the velocity of light. Assuming the typical JET plasma pedestal widths to be within the range (2-5)cm, the minimum required sampling interval should be ≤1cm. This requirement is just provided here by the block 1 in figure 3. In the Core LIDAR the same requirement is expected to be fulfilled (as mentioned above) by the hardware upgrade of the detection & acquisition system (20 GHz sampling frequency, corresponding to Δr=0.75 cm). In this case the use of the block 1 for transformation to new sampling steps in figure 3 will be avoided (dashed line in figure 3).

4. ALGORITHM FOR TRANSFORMATION TO A NEW SAMPLING STEP

Another possibility to obtain more detailed description of the pedestal area is to apply some

specific software transformations of standard Core LIDAR profiles to a new sampling step. The attractiveness of such an approach is that it does not require hardware modifications of the LIDAR system and provides an opportunity to analyze the performance of the main algorithm (block 2) using the present data. It must be noted that any interpolation techniques for transformation to a finer step are not eligible to be applied to Core LIDAR data, mainly because the processing chain assumes the application of deconvolution. The well known fact that the interpolation does not provide any new information is realized in the presence of zero spectral components in the instrument function, i.e., $R_{lid}(\omega) = 0$ for frequencies $\omega_N \le \omega \le \omega_{new}$, higher that the Nyquist frequency ω_N of standard Core LIDAR data, $\omega_{new} = \pi/\delta r$ is the Nyquist frequency, corresponding to the new step $\delta r < \Delta r$ after the transformation. This fact imposes strong limitations on the choice of the transformation method in the block 1 in figure 3.

In this work the above problem is solved by applying our original algorithm for transformation to finer sampling steps, developed earlier for processing of 1D and 2D signals and described in details in [14,15]. The transformation method is not based on interpolation techniques. The spectral components of the instrument function are nonzero or $R_{lid}(\omega) \neq 0$ for $\omega_N \le \omega \le \omega_{new}$. This algorithm was tested in many experiments with real sampled data. It was clearly demonstrated that the algorithm is eligible for problems, containing deconvolution. Below we will analyze the requirements to and some limitations of the method in the sense of its application to the problem of estimation of the true pedestal from Core LIDAR data (see the Appendix that contains a description of the method).

The requirements to the method application were preliminary checked by different criteria for all processed plasma pulses. The first one requires stationary LIDAR profiles for intervals for at least several (3-4) laser shots. Our analysis of LIDAR profiles during the H-mode shows that this requirement is well fulfilled. This is demonstrated in figure 4a for the JET Pulse No: 73334, where the appearance of the H-mode is well seen. Here, the total areas of the six Core LIDAR profiles as a function of the shot number are given. It is seen that within the H-mode the total LIDAR profile areas are fluctuating around some well defined mean values without trends. The variations of the mass center positions of LIDAR profiles within the pedestal area (responsible for formation of electron temperature & density pedestals) are shown in figure 4b. Their behavior also displays good stationary processes with variances ~ (0.2-0.4) of the sampling step. The origin of these fluctuations is mainly due to signal noises. Other parameters that cause the signal to vary are central sawteeth and Edge Localized Modes (ELMs). In this analysis the data is averaged over the sawteeth and ELMs. Future analysis on the upgraded LIDAR system will resolve these events.

The next requirement is the presence of some reference signal of width that is considerably larger than the sampling step [14,15]. This is also fulfilled, considering each LIDAR profile as a whole (including the pedestal) in each channel as the reference signal as it contains about 60 pixels. The short pedestal is assumed as a short non-resolved signal firmly fixed to the reference signal (LIDAR profile).

Therefore, the basic requirements to the application of the method given in details in the Appendix are fulfilled. The operation of the algorithm in block 1 is based on the lack of synchronization between the laser pulse and the ADC sampling generator, resulting in some time delays within one sampling step of the acquired LIDAR profiles with respect to the laser emission. These delays, containing information for the fine structure of LIDAR profiles (such as the pedestal) are estimated by the algorithm from the sampled LIDAR data. Then, the LIDAR profiles are rearranged on the finer time scale, taking into account the above time delays preliminary divided into Q groups (Q is the transfer ratio from the present sampling step to the new one). For $Q = 3$, for example, the new sampling step δr will be equal to $\delta r = \delta r/Q = 1$ cm.

The transformation is applied only once to the recorded LIDAR profiles. As a result of the transformation one will obtain a set of transformed convolved profiles $L_p^{tr\_con}(r)$. Next, we will define (for simplicity) the discretized forms of the LIDAR profiles $L_p^{con}(r)$ and $L_p^{tr\_con}(r)$ as

$$\begin{cases} L_p^{con}(k) = L_p^{con}(k\Delta r) \\ L_p^{con}(j) = L_p^{tr\_con}(j\delta r) \end{cases}$$

where $k \in [1, K_{jet}]$ and $j \in [1, J]$, with $K_{jet} = L_{torus}/\Delta r$, $J = K_{jet}Q$; L_{torus} is a torus length. Below the two integers k and j will be used to denote and distinguish the original (registered) and the transformed LIDAR profiles. In this study we accepted for the transfer ratio to be equal to $Q = 3$. The minimum number of shots for $Q = 3$ is of the order of 4 (see the Appendix).

It is important to note that the transformed profiles $L_p^{con}(j)$ do not contain any interpolated values.

The transformed deconvolved profiles $L_p^{dcv}(j)$ can be calculated using the instrument function, but also transformed to the new time scale. In this study we applied the same approach [14,15] to the extraction of the transformed instrument function $R_{lid}(j)$, using a computer model based on some well known models of the partial functions $R_{adc}(j)$, $R_{det}(j)$ and $R_{las}(j)$.

The application of the transforming algorithm to Core LIDAR profiles is demonstrated in figure 5, where the mean LIDAR profiles over the H-mode are presented. As seen, the original (convolved & deconvolved) profiles (JET Pulse No: 73344) of step $\Delta r_{jet} = 3$cm of 5 GSa frequency (figures 5(*a*) and 5(*c*), respectively) are similar to those after the transformation (figures 5(*b*) (convolved) and 5(*d*) (deconvolved), respectively). Their temporal interpositions are saved after the transformation. Moreover, the deconvolution of transformed profiles (1cm step) is also of good quality as for the original deconvolved profiles (3 cm step). It may be concluded that the transformed profiles could be used for further application of the algorithm for estimation of the true pedestal in the new sampling scale $\Delta r = 1$ cm of equivalent sampling frequency of 15GHz.

5. OPTIMAL ALGORITHM FOR ESTIMATION OF THE ELECTRON TEMPERATURE PEDESTAL FROM JET CORE LIDAR DATA.

We will introduce the following basic parameters of the electron temperature pedestal, concerned

in the optimal algorithm below described: 1) The normalized shape of the pedestal function $S_{ped}^{norm}(j)$ (because of the low number of samples within the pedestal area, the description & extraction of this function is not so unambiguous and accurate). For simplicity we are accepting here the pedestal function $S_{ped}(j)$ to be preliminary chosen. In our analysis we used two kinds of pedestal functions: a cosine function in the interval $(0-\pi)$ and a linear function; 2) The pedestal amplitude A_{ped}; 3) The pedestal width W_{ped}, defined in a number j_w of sampling steps $W_{ped} = j_w \delta r$; 4) The upper position r_{ped} of the pedestal function (also defined in sampling steps $r_{ped} = j_r \delta r$). The pedestal shape of a cosine-type (mainly used in calculations), containing the above parameters is given by the expression

$$S_{ped}(j) = A_{ped}\,[(1\text{-}cos(\pi(j_r + j_w - j) / j_w))/2],\ 0 \le j < j_w \quad .$$

The algorithm for estimation of the true electron temperature pedestal is the key algorithm here. Its more detailed block-schematic is shown in figure 6. The basic idea here is in creation of a model of some electron temperature profile $T_e^{var}(j)$ of variable pedestal characteristics defined through the pedestal parameters: $S_{ped}^{norm}(j)$, A_{ped}, W_{ped} and r_{ped}. Outside the pedestal area we assumed the electron temperature profile to be equal to the convolved profile $T_e^{con}(j)$. The last is assumed to be retrieved from the transformed LIDAR profiles $L_p(j)$, $p = 1..6$ using the TS relativistic spectra [16-18].

It can also be shown (following the expression in (6) for the links of the deconvolved and true LIDAR profiles) that a similar relation is existing between the deconvolved electron temperature profiles $T_e^{dcv}(j)$ and the electron temperature profiles $T_e^{true}(j, H(j))$, retrieved from the set of true LIDAR profiles $L_p^{true}(j)$ after their convolution in (6) with the LPF characteristic $H(j)$ or:

$$T_e^{dcv}(j) = T_e^{true}(j, H(j)) \quad . \tag{7}$$

To show this fact, let us use the method of mass-centre, developed in [18,19] for retrieving the electron temperature. It is based on the unambiguous dependence $\lambda_{mass}(T_e) = f(T_e)$ of the mass-centre position λ_{mass} of the recorded relativistic TS spectra on the temperature T_e. This dependence was successfully applied to retrieve the T_e profiles from Core LIDAR data (convolved & deconvolved). Really, the mass-centre λ^H_{mass} of the convolved by $H(j)$ true LIDAR profiles $L_p^{true}(j)$ is expressed by

$$\lambda^H_{mass}(T_e(j, H(j))) = \frac{\sum_p \lambda_p L_p^{true}(j) \otimes H(j)}{\sum_p L_p^{true}(j) \otimes H(j)}\ , \tag{8}$$

where λ_p is the mass-center of the TS radiation received in the *p-th* channel, shaped by the spectral transmissions of the corresponding optical receiving blocks. Using now the expression in (6) into the right-hand side of (8) one will obtain that

$$\lambda^{dcv}_{mass}(T_e^{dcv}(j)) = \lambda^H_{mass}(T_e(j, H)(j))) \tag{9}$$

for each distance j inside the torus. Because of the unambiguous dependence $\lambda_{mass}(T_e) = f(T_e)$ the equality in (7) is also fulfilled.

The input profiles for the algorithm in the block 2 in figure 3 are the convolved $T_e^{con}(j)$ and the deconvolved $T_e^{dcv}(j)$ electron temperature profiles, retrieved in the finer sampling step from transformed convolved $L_p^{con}(j)$ and deconvolved $L_p^{dcv}(j)$ LIDAR profiles. The next step is the preliminary estimation of the approximate pedestal upper position r_{ped}. To this purpose let us consider the behaviour of the convolved and deconvolved temperature profiles in the pedestal area using the modelled electron temperature profiles shown in figure 2. As seen, both the convolved and deconvolved profiles are close to each other inside the torus. This can be explained by the residual convolution of the low-pass filter and the lower as a rule amplitudes & steepness of temperature inhomogeneities (with respect to the pedestal) inside the torus. The pedestal can also be considered as an ingredient of amplitudes & steepness larger than the in-torus inhomogeneities. As a result, both the convolved and deconvolved profiles are obtained significantly different (split) just into the pedestal area. This difference (and thus, the splitting) is due mainly to the deconvolved profiles because of the improved resolution. The upper position r_{ped} of the pedestal function is disposed just in the beginning of the splitting area marked with a circle in figure 2. This fact can be used to obtain a preliminary estimate $\tilde{r}_{ped} = \tilde{j}_{ped}\delta r$ of r_{ped}. The estimate $\tilde{j}_{ped}$ can be calculated by the expression

$$T_e^{con}\left(\tilde{j}_{ped}\right) - T_e^{dcv}\left(\tilde{j}_{ped}\right) \sim TrSh * \left[T_e^{con}\left(\tilde{j}_{dcv}\right) - T_e^{dcv}\left(\tilde{j}_{dcv}\right)\right] \tag{10}$$

where $TrSh$ is some threshold, typically $TrSh \sim (0.1\text{-}0.3)$; the value of $\tilde{j}_{ped}$ is determined by the conditions $T_p^{dcv}(j_{dcv}) > 0$ and $T_e^{dcv}(\tilde{j}_{dcv} + 1) = 0$ (see figure 2). Here and in what follows, the notation "~" will mean an estimate of the corresponding function or parameter.

The next step is the creation of a variable model $T_e^{var}(j)$ of the electron temperature profile, according to the expressions:

$$T_e^{\mathrm{var}}\left(j\right) = \begin{cases} T_e^{con}\left(j\right) & for \quad j \le \tilde{j}_{ped} \\ A_{ped} S_{ped}^{norm}\left(\tilde{j}_{ped} + j_W - j\right) & for \quad \tilde{j}_{ped} < j \end{cases}. \tag{11}$$

In (11) we accepted the electron temperature profile $T_e^{var}(j)$ inside the torus to be determined by the convolved profiles $T_e^{con}(j)$ in the finer step (one could also use the deconvolved profiles $T_e^{dcv}(j)$ as well). We have chosen the convolved profiles because of two reasons: i) the convolved profiles are less affected by noise; ii) the pedestal area is of basic interest in this analysis, while the resolved electron temperature variations inside the torus are already determined by the deconvolution.

Then we have to take into account the effect of LPF characteristic $H(j)$ on the variable electron temperature profile $T_e^{var}(j)$ and thus, to obtain the convolved with $H(j)$) variable electron temperature profile $T_e^{var}(j, H(j))$. To this purpose we have to decompose the input variable profile $T_e^{var}(r)$ into 6-chanels variable LIDAR profiles $L_p^{var}(j)$, using also a model of an electron density profile $n_e^{var}(j)$.

In this study we accepted the variable electron density model $n_e^{var}(j)$ to be defined by

$$n_e^{\mathrm{var}}(j) = \begin{cases} 1 \quad for \quad j \le \tilde{j}_{ped} \\ S_{ped}^{norm}\left(\tilde{j}_{ped} + j_W - j\right) \quad for \quad \tilde{j}_{ped} < j \end{cases} . \tag{12}$$

As seen, it is accepted for the electron density to be defined by the same pedestal function as the electron temperature pedestal. The electron density $n_e^{var}(j)$ inside the torus is accepted to be constant and equal to unity in order to avoid some unwanted amplitude shifts in $T_e^{var}(j, H(j))$ after the back composition. This choice of $n_e^{var}(j)$ was preliminary tested by simulations, using independently variable pedestal function. The simulations show that the best algorithm performance is realized when both the pedestal functions are similar. That is why we used in this study the model in (12) for all cases of processing of real Jet Core LIDAR data. The good coincidence of the estimated electron temperature pedestals by both the Core LIDAR and HRTS instruments is also some criterion for the choice of $n_e^{var}(j)$ according to (12).

The next intermediate procedures are the convolution of variable LIDAR profiles $L_p^{var}(j)$ with the LPF characteristic $H(j)$, presented by

$$L_p^{\mathrm{var}}\left(j, H\left(j\right)\right) = L_p^{\mathrm{var}}\left(j\right) \otimes H\left(j\right) \ , \ p = 1..6 \ . \tag{13}$$

Then, using the mass centre algorithm [18,19] or the fitting algorithm [20] one can restore the convolved variable electron temperature profile $T_e^{var}(j, H(j))$ or

$$\left\{ L_p^{\mathrm{var}}\left(j, H\left(j\right)\right), p = 1..6 \right\} \Rightarrow T_e^{\mathrm{var}}\left(j, H\left(j\right)\right)$$

Using now the calculated profiles $T_e^{dcv}(j)$ and $T_e^{var}(j, H(j))$ of given pedestal characteristics one can calculate the functional F_{lsf}, defined by

$$F_{lsf} = \sum_{j \in ped.area} \left[T_e^{dcv}\left(j\right) - T_e^{\mathrm{var}}\left(j, H\left(j\right)\right) \right]^2 . \tag{14}$$

The above expression is based on the equation (7). As it is seen this is an application of the well known least square method, where the convolved variable temperature profile $T_e^{var}(j, H(j))$ is compared with the deconvolved profile $T_e^{dcv}(j)$ within the pedestal area. According to (7) the functional F_{lsf} has a minimum (because of noises) when $T_e^{var}(j, H(j)) \rightarrow T_e^{true}(j, H(j))$ within the pedestal area. The profile $T_e^{var}(j)$ with pedestal parameters, corresponding to the minimum of the functional F_{lsf} in (14) is accepted as an estimate of the true electron temperature profile. As is well known, the problem formulated by the expression in (14) provides an optimal estimate of the electron temperature profile. Then, after finding the optimal pedestal parameters one can restore the total electron temperature profile in the torus over the entire sounding path, including the more detailed information about the plasma pedestal.

At given pedestal shape the functional in (14) depends on the three pedestal parameters A_{ped}, W_{ped} and r_{ped}. Therefore, the functional F_{lsf} describes a 3-dimensional fitting procedure for determination of the best fit (the estimate $T_e^{true}(j)$) to the true electron temperature profile. The pedestal parameters are defined in proper numbers of steps and varied within their tolerable limits:

$$A_{ped}\left(j_a\right) = A_0 T_e^{dcv}\left(j_{ped}\right)\left(j_a / J_A\right),\ j_a = 1..J_A \tag{15a}$$

$$W_{ped}\left(j_W\right) = j_W \delta r,\ j_W = 1..J_W,\ J_W \geq \left(j_{dcv} - \tilde{j}_{ped}\right) \tag{15b}$$

$$j_{ped}\left(j_r\right) = \tilde{j}_{ped} + j_r\ ,\ \ j_r = -J_r^I ... J_r^{II}\ , \tag{15c}$$

where j_a, j_W and j_r are the corresponding integer variable parameters for the pedestal amplitude, width and upper position, respectively; J_A, J_W, J_r^I and J_r^{II} are their corresponding limits of variations. As a result, the positive values of the functional $F_{lsf}(j_a, j_W, j_r)$ in (14) depend on the integer pedestal parameters. After passing the full set of variations of integer parameters $\{j_a, j_W, j_r\}$ within the ranges defined in (15a-15c), one will obtain a set of values for the functional F_{lsf} given by $\{F_{lsf}\ (j_a, j_W, j_r)\}$. Then, the minimal value $(F_{lsf}\ (j_a^{\ min}, j_W^{\ min}, j_r^{\ min}))_{min}$ of the functional F_{lsf} can be determined, where the values of arguments $j_a^{\ min}, j_W^{\ min}$ and $j_r^{\ min}$ correspond to the minimal value of the functional F_{lsf}. Thus, the optimal estimate of the pedestal cos-type function can be now directly determined as

$$S_{ped}^{fit}\left(j\right) = A_{ped}^{\min}\left(j_a^{\min}\right)\cos\left(\pi\left(j_r^{\min} + j_W^{\min} - j\right)\Big/ j_W^{\min}\right) \tag{16}$$

where $A_{ped}^{min}(j_a^{\ min})$, $j_W^{\ min}$ and $j_r^{\ min}$ can be directly calculated from (15a-c) at known parameters $j_a^{\ min}$, $j_W^{\ min}$ and $j_r^{\ min}$. Finally, the entire torus electron temperature profile $\tilde{T}_e^{true}(j) = T_e^{min}(j)$ with the resolved pedestal within the torus is given by

$$\tilde{T}_e^{true}\left(j\right) = \begin{cases} T_e^{con}\left(j\right) & for \quad j \leq j_{ped} \\ S_{ped}^{fit}\left(j\right) & for \quad j_{ped} < j \leq j_{wall} \end{cases} \tag{17}$$

This is the final result of the algorithm chain – to recover the full electron temperature profile along the line of sight inside the torus, containing the resolved pedestal. The good coincidence (see below figure 7b) of $T_e^{min}(j, H(j))$ and $T_e^{dcv}(j)$ in the pedestal area also supports the correctness of the full processing chain, including the transformation to a new sampling step, the residual convolution with the low pass filter $H(j)$, etc.

6. SIMULATIONS

The method performance (including the transformation to the new sampling step of 1cm) was preliminary analyzed by simulations, using a computer model based on the present Core TS

LIDAR parameters. As input data we used models of the electron temperature profiles $T_e^{var}(j)$ of variable pedestal parameters $S_{ped}^{norm}(j)$, A_{ped}, W_{ped} and r_{ped} defined with a sampling step δr = 1cm. They are further used for comparisons with the processed pedestal parameters. Then, the modeled LIDAR data (step Δr = 3cm) that are input to the processing chain in figure 3 are obtained by a decimation with a factor $Q = 3$. The transfer from plasma parameters – the electron temperature $T_e^{var}(j), T_e^{var}(k)$ and the electron density $n_e^{var}(j), n_e^{var}(k)$ profiles of steps 1cm and 3cm, respectively, to the corresponding LIDAR profiles is performed by using the Thomson scattering relativistic spectra [16-18]. The signal-to-noise ratio (*SNR*) in the LIDAR profiles is of essential importance for the quality of the output data and thus, for the method performance. Therefore, we preliminary estimated the *SNRs* in the real LIDAR profiles. In principle, the *SNRs* are different in different channels, depending on many well known factors. In general, the typical maximum electron temperatures near the torus center vary within the range of 3.5-7keV. The highest signal magnitude maxima in LIDAR profiles (after anti-vignetting) are obtained in the 3rd and the 4th spectral channels. Moreover, the *SNRs* in other channels are mutually linked through the $T_e(r)$ and $n_e(r)$ profiles, TS relativistic spectra and the spectral channel parameters. Following these arguments we defined the *SNR* as a ratio of the mean LIDAR profile maximum (over the H-mode) in the 4-th channel to the mean square value σ_{noise} of the total noises (Poisson and Gaussian) at the corresponding LOS distance. Analyzing the data we found that this *SNR* is of the order of 20. Following this definition of the *SNR* we performed simulations for *SNRs* = 40, 20 and 10. The number I of processed laser shots (within the JET pulse) was chosen to be $I = 25$ (typical for the H-mode in high triangularity plasma). Then, at given $T_e(r)$, $n_e(r)$ profiles we created sets of I groups each of 6 LIDAR profiles corresponding to the 6 spectral channels of the Core LIDAR to be further analyzed by the algorithms developed.

The examples of input variable $T_e^{var}(j)$ profiles (1 cm step) for two different pedestal parameters are shown in figure 7a. At fixed wall position the pedestal widths (0.1-0.9 levels) were varied within the range from 1.8cm to 5cm at pedestal amplitudes ~ 1KeV that are typical for JET plasma. The profiles of plasma electron temperatures inside the torus were chosen as typically accepted in JET Core LIDAR simulations. The processing chain is strictly following the algorithms in figure 2 and figure 6. The performance of the fitting procedure (see also Sec.7) is demonstrated on the figure 7b. Here curve 1 shows the input (true) $T_e^{true}(j)$ profile and curves 2 and 3 show the convolved $T_e^{con}(j)$ and the deconvolved $T_e^{dcv}(j)$ profiles in 1cm-sampling step, respectively. As seen, when the retrieved estimate $\widetilde{T}_e^{true}(j)$ (curve 4) of the input profile is closely coincident with $T_e^{true}(j)$ (curve 1) within the pedestal area, then the profile $\widetilde{T}_e^{true}(j)$ convolved by $H(r)$ profile - $\widetilde{T}_e^{true}(j,H(j))$ (curve5) is overlapped well on $T_e^{dcv}(j)$ (curve 3).

Statistical results over a defined set of simulations for *SNR* = 20 are presented in figures 8a,b,c. The deviations of the retrieved pedestal widths for input pedestal widths ranging from 1.8cm to 5cm are given in figure 8a. It can be seen that the retrieved pedestal widths vary by ±1cm with respect to the input pedestal widths. Then, the deviations of the pedestal amplitudes of retrieved

estimates $\widetilde{T}_e^{true}(j)$ for input pedestal amplitudes are given in the next figure 8b. As seen, the output pedestal amplitudes vary within the range of 0.2keV (from 0.8KeV to 1.0keV) at input amplitude variations (at different pedestal widths) of 0.1keV.

The plot in figure 8c displays the variations of pedestal positions of retrieved estimates of the true profiles $\widetilde{T}_e^{true}(j)$ with respect to the true pedestal positions of input profiles. We accepted here the corresponding positions of the pedestal levels at 0.1 and 0.9 of the pedestal amplitude as definitions of the lower and upper pedestal positions, respectively, as these parameters are easier for determination. The input pedestal widths (0.1-0.9 levels) are plotted on the x-axis for 8 discrete values from 1.8cm to 5cm. The position of the torus wall is also marked on the plot. Moreover, the dependences of the lower (0.1) and the upper (0.9) true pedestal positions (curves 1 and 2, respectively) as functions of their widths are also given. As seen, both the pedestal positions are shifted away from the wall for larger widths. The variations of both the lower and upper pedestal positions determined by the method vary around the corresponding true pedestal positions. A part of the lower pedestal positions are retrieved outside the wall (negative positions) for shorter widths. Some very limited number of negative lower positions is obtained for larger widths as well. The appearance of negative positions can be explained by the effects of noises and low number of samples per a pedestal width. It can be expected that these effects could be minimized by increasing the *SNR* of LIDAR profiles (3 times) and using shorter sampling step (0.75cm) as expected from the upgrade of the Core LIDAR system.

The simulation results confirm the tolerable performance of the method at system parameters, typical for the present JET Core LIDAR data (*SNRs* ~ 20, step 3cm). The variations of the retrieved pedestal parameters are larger for lower *SNRs* ~ 10. Such *SNRs* are realized some times in the low-triangularity JET pulses of low electron densities. In general, the method application at *SNRs* ~ 10 and below can be accepted as intolerable. The simulations also confirm the good method performance at higher *SNRs*, say *SNRs* ~ 40 and more. This very important fact can be further used as a starting point for simulation analyses of method applications in the upgraded JET Core LIDAR as well as in the ITER Core LIDAR.

7. APPLICATION TO REAL JET CORE LIDAR DATA

We will present now the experimental results from the application of the entire processing chain, according to the algorithms in Secs.3-5 to the real Core LIDAR data (3cm step) from a defined set of JET pulses. The plots in figure 9 display the estimated profiles $\widetilde{T}_e^{true}(r)$ of a step 1cm, retrieved from the mean LIDAR profiles, averaged (according to the algorithm in Sec.4) over the H-mode. The JET pulses processed (Pulse Nos: 73340, 73346 and 73347) are of high triangularity type. The input pedestal shape is of cos-type. As seen, the electron temperature pedestals in the wall vicinity are now well defined by a step 1cm with respect to the torus wall after the application of the fitting algorithm in Sec.5. The use of a linear pedestal shape was not so good as it was by the cos-type model. As seen, the retrieved electron temperature pedestals are also well defined by a step 1cm

with respect to the torus wall after the application of the fitting algorithm. We note that for some set of JET pulses of very low electron densities, the application of the method was not successful and these pulses were not included. The use of the method in such cases requires further improvement of the processing algorithm. Using the method developed one can create now the total electron temperature profile, containing both the resolved pedestal and the profile inside the torus with a finer step of 1cm (figure 10). The plots in figures 9-10, presenting the mean (over the H-mode) resolved electron temperature profiles are averaged typically over 20-30 successive shots.

The presented experimental results from processing the real TS Core LIDAR data demonstrate the good performance of the method developed for estimation by software techniques alone of the true electron temperature pedestal parameters (shape, width, amplitude, position) as well as the entire electron temperature profile in the torus with a finer sampling step. If combined with the improved quality of the LIDAR signal after the expected upgrade of the receiving & digitizing system, this method can provide detailed information (in time and space) about the pedestal parameters of JET plasma, being well compatible with future ITER Core LIDAR as well.

CONCLUSIONS

We developed and tested by simulations and by real data processing a novel method for estimation of the true electron temperature pedestal from JET Core LIDAR profiles. Its application to present LIDAR data requires preliminary transformation of original LIDAR profiles (3cm sampling step) to a new sampling scale of 1 cm step. Then we applied a three-parameter optimal least-square algorithm to extract the best fit of the electron temperature pedestal parameters at a given pedestal shape. As a result, we retrieved the true electron temperature profile over the entire plasma diameter, containing the resolved pedestal. The simulation analysis by a computer model, based on the TS Core LIDAR parameters, demonstrates the expected performance of the full processing algorithm based on the novel method.

The algorithm is used to process a set of data from different pulses for plasmas of high triangularity to demonstrate the method on real data. The resolving of the electron temperature pedestal from Core LIDAR data (demonstrated for the first time in this work) contributes to the increasing of the information quality of the plasma diagnostics on JET. The novel method & algorithms are appropriate for processing the JET Core LIDAR data (especially with the upgraded system) as well as with the future ITER Core LIDAR data.

ACKNOWLEDGEMENTS

This work, carried out within the framework of the European Fusion Development Agreement, has been supported by the European Communities under the Contract of Association between EURATOM and INRNE (Bulgaria) and by the Bulgarian National Science Fund under the contract DO 02-107/2009. The views and opinions expressed herein do not necessarily reflect those of the European Commission.

APPENDIX

TRANSFORMATION OF CORE LIDAR PROFILES TO A FINER SAMPLING STEP

Let us denote the original convolved LIDAR profiles are sampled with a step Δr = 3cm by $L_{i,p}^{con}(k\Delta r)$, where $i = 1..I_t$ is the number of successive laser shot, I_t is the total number of processed shots within the plasma pulse, p= 1..6 is the number of spectral channel, $k = 1..\ K_{jet} = L_{torus}/\Delta r >> 1$ is the torus length L_{torus} in a number of sampling steps; kΔr is the discrete distance along the sounding path, $K_{jet} \sim 60$. In further consideration we will follow the description of the method in [14,15].

As mentioned in Sec.4 the transformation method rearranges the samples of some set of $I < I_t$ successive LIDAR profiles $L_{i,p}^{con}(k)$ in the p-th channel to a single transformed LIDAR profile $L_p^{tr\_con}(j)$ of finer sampling step $\delta r = \Delta r/Q$; $j = 1..\ J, j = \mathrm{K}_{jet}\mathrm{Q}$, Q = $\Delta r/\ \delta r$ is an integer, noted as a transfer ratio. The information for the rearranging is extracted by calculation of the additional time delays δt_{samp} of each LIDAR profile $L_{i,p}^{con}(k)$ due to the lack of synchronization of the ADC sampling instants with respect to the ADC start (synchronized with the laser emission). As a result, the sampling instants (and thus, the sampled LIDAR profiles) are delayed additionally within the range of a single sampling interval ($0 \le \delta t_{samp} < \Delta t = 2\Delta r/c'$).The sampling interval Δt can be divided into a set of successive subintervals of delays $\delta t_l = (l\text{-}1)\delta t$, $l = 1..Q$ and of length $\delta t = \Delta t/Q$. The algorithm provides estimations of additional delays δt_{samp} of each LIDAR profile, determining its belonging to the corresponding subinterval δt_l and then rearranging the LIDAR profile samples, according to the estimates of $\delta r_l = \mathrm{c}\delta t_l/2$.

For this purpose we will define a new LIDAR profile time series $U_{i,p}(j)$ in a new time scale of step δr, where the positions of LIDAR samples $L_{i,p}^{con}(k)$ inside the step Δr are determined by the rule $j\delta r = k\Delta r + \delta r_l$, $k = 1..\ K_{jet}$, $l = 1..Q, j = 1..J, J = K_{jet}Q$:

$$U_{i,p}(j) = \begin{cases} L_{i,p}^{con}(k) & for \quad j = kQ + round\left[j_R - (j_{mass})_{i,p}\right] \\ 0 & for \quad j \neq kQ + round\left[j_R - (j_{mass})_{i,p}\right] \end{cases} \tag{1A}$$

where $(j_{mass})_{i,p}$ is the mass center of $U_{i,p}(j)$ in numbers of new steps δr; j_R is some reference point, the same for all the processed data, chosen as a rule arbitrary on the new time scale. It is evident that the delays $\delta r_l = \mathrm{c}\delta_t/2$ are included into the mass center estimate $(j_{mass})_{i,p}$ as it defines the total delay of the new LIDAR profile $U_{i,p}(j)$ in (1A). The values of the transformed LIDAR profile $L^{tr\_con}(j)$ are obtained by the same expression [14,15]:

$$L_p^{tr\_con}(j) = \begin{cases} \sum_i^I U_{i,p}(j) \Big/ \sum_i^I m_{i,p}(j) \\ \quad for \quad \sum_i^I m_{i,p}(j) > 0, \\ 0 \quad for \quad \sum_i^I m_{i,p}(j) = 0, \end{cases} \tag{2A}$$

where the integer time series $U_{i,p}(j)$ is given by

$$m_{i,p}\left(j\right) = \begin{cases} 1 & for \quad j = kQ + round\left[j_R - \left(j_{mass}\right)_{i,p}\right] \\ 0 & for \quad j \neq kQ + round\left[j_R - \left(j_{mass}\right)_{i,p}\right] \end{cases} \tag{3A}$$

The last series is accounting for cases, when more than one of the LIDAR profiles have the same estimates of the additional delays δr_l. In such cases the algorithm provides averaging of transformed LIDAR profiles $U_{i,p}(j)$ in the new transformed profile. It must be noted that the noises in adjacent new sampling intervals are non-correlated as they are created by LIDAR profiles from different shots. The minimum number of profiles (shots) is given by the condition $I_{min} > Q$. In the last case there is practically no averaging in the transformed LIDAR profiles and thus, the *SNR* of signals in $L_p^{tr\_con}(j)$ is of the same order as of the original profiles $L_{i,p}^{con}(j)$.

REFERENCES

[1] Salzmann H, Bundgaard J, Gadd A, Gowers C, Hansen K.B, Hirsch K, Nielsen P, Reed K, Schrödter C and Weisberg K 1988 *Review of Scientific Instruments* **59** 1451

[2] Kempenaars M, Balboa I, Beurskens M, Flanagan J.C. and Maslov M 2010 *Int. Conference on Plasma Diagnostics*, Pont-à-Mousson, France, 12-16 April, paper P30.

[3] Kempenaars M, Flanagan J C, Giudicotti L, Walsh M J, Beurskens M and Balboa I, 2008 *Review of Scientific Instruments* **79** 10E728

[4] Gowers C, Beurskens M and Nielsen P 2000 *Journal of Plasma Fusion Results* **76**, 874

[5] Pasqualotto R, Nielsen P, Gowers C, Beurskens M, Kempenaars M, Carlstrom T and Johnson D 2004 *Review of Scientific Instruments* **75** 3891

[6] Kempenaars M, Nielsen P, Pasqualotto R and Gowers C 2004 *Review of Scientific Instruments* **75**, 3894

[7] Gurdev L, Dreischuh T and Stoyanov D 1993 *Journal of the Optical Society of America A* **10** 2296

[8] Amini A.M, 1995 *Applied Optics* **34** 1878

[9] Dreischuh T, Gurdev L and Stoyanov D 1995 *Journal of the Optical Society of America A* **12** 301

[10] Bahrampour A.R and Askari A.A 2006 *Optics Communication* **257** 97

[11] Refaat T.F, Ismail S, Abedin M.N, Spuler S.M and Singh U N 2008 *Applied Optics* **47** 5281

[12] Stoyanov D, Dreischuh T, Gurdev L, Beurskens M, Ford O, Flanagan J, Kempenaars M, Balboa I and Walsh M 2009 *ECA* 33E P-2.155 (European Physical Society, Geneva, 2009), ISBN:2-914771-61-4

[13] Dreischuh T, Gurdev L and Stoyanov D 2011 *Proc. SPIE* 7747 77470T.

[14] Stoyanov D, Dreischuh T, Vankov O and Gurdev L 2004 *Measurement Science and Technology* **15** 2361

[15] Stoyanov D, Nedkov I and Ausloos M 2007 *Journal of Microscopy* **226** 270
[16] Naito O, Yoshida H and Matoba T 1993 *Physics of Fluids* B**5** 4256
[17] Selden A C 1980 *Physics Letters* **79**A 405
[18] Gurdev L, Dreischuh T and Stoyanov D 2008 *Proc. SPIE* 7027 702711
[19] Dreischuh T, Gurdev L, Stoyanov D, Beurskens M, Walsh M and Capel A 2009 *ECA* 33E P-2.149 (European Physical Society, Geneva, 2009), ISBN:2-914771-61-4
[20] Mattioli M and Papoular R 1975 *Plasma Physics* **17**, 165
[21] Stoyanov D, Beurskens M, Dreischuh T, Gurdev L, Ford O, Flanagan J, Kempenaars M, Balboa I and Walsh M, 2010 *ECA* 34A P-5.133 (European Physical Society, Geneva, 2010), ISBN 2-914771-62-2

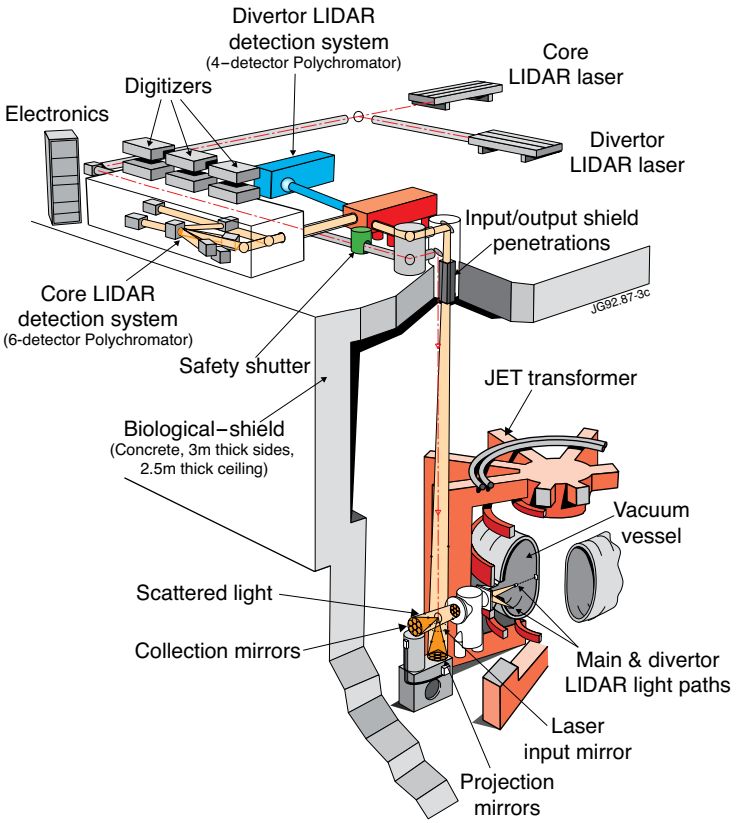

Figure 1: JET LIDAR Thomson scattering diagnostic system.

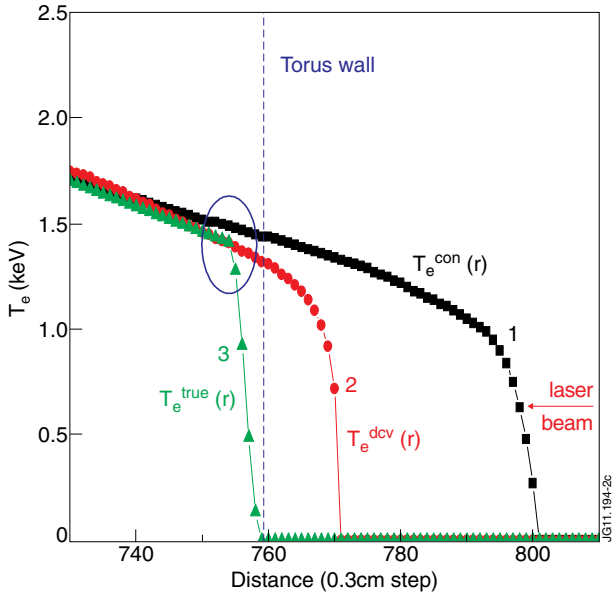

Figure 2: Behavior of the electron temperature profiles in the pedestal area: convolved T_e^{con} (r) (curve 1), deconvolved T_e^{dcv} (r)(curve 2) and the input true T_e^{true} (r)(curve 3) profiles. The position of the torus wall is also marked (dashed line).

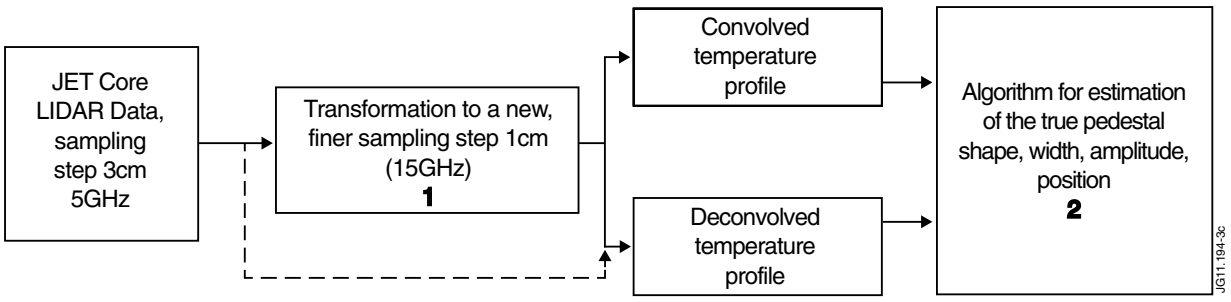

Figure 3: General block-schematic of the entire processing chain.

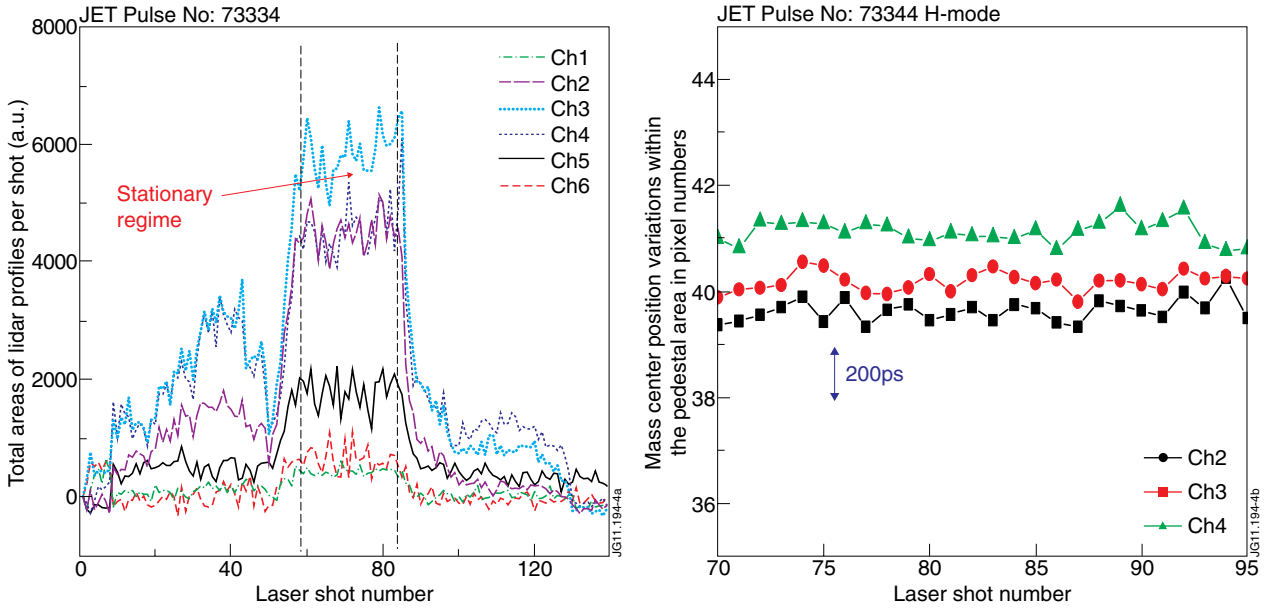

Figure 4: (a) The temporal history of the total areas (along the torus radius) of the six Core LIDAR profiles as a function of the shot number for plasma Pulse No: 73334. (b) The variations (from shot to shot) of the mass center positions of LIDAR profiles in different channels within the pedestal area (responsible for formation of electron temperature and density pedestals).

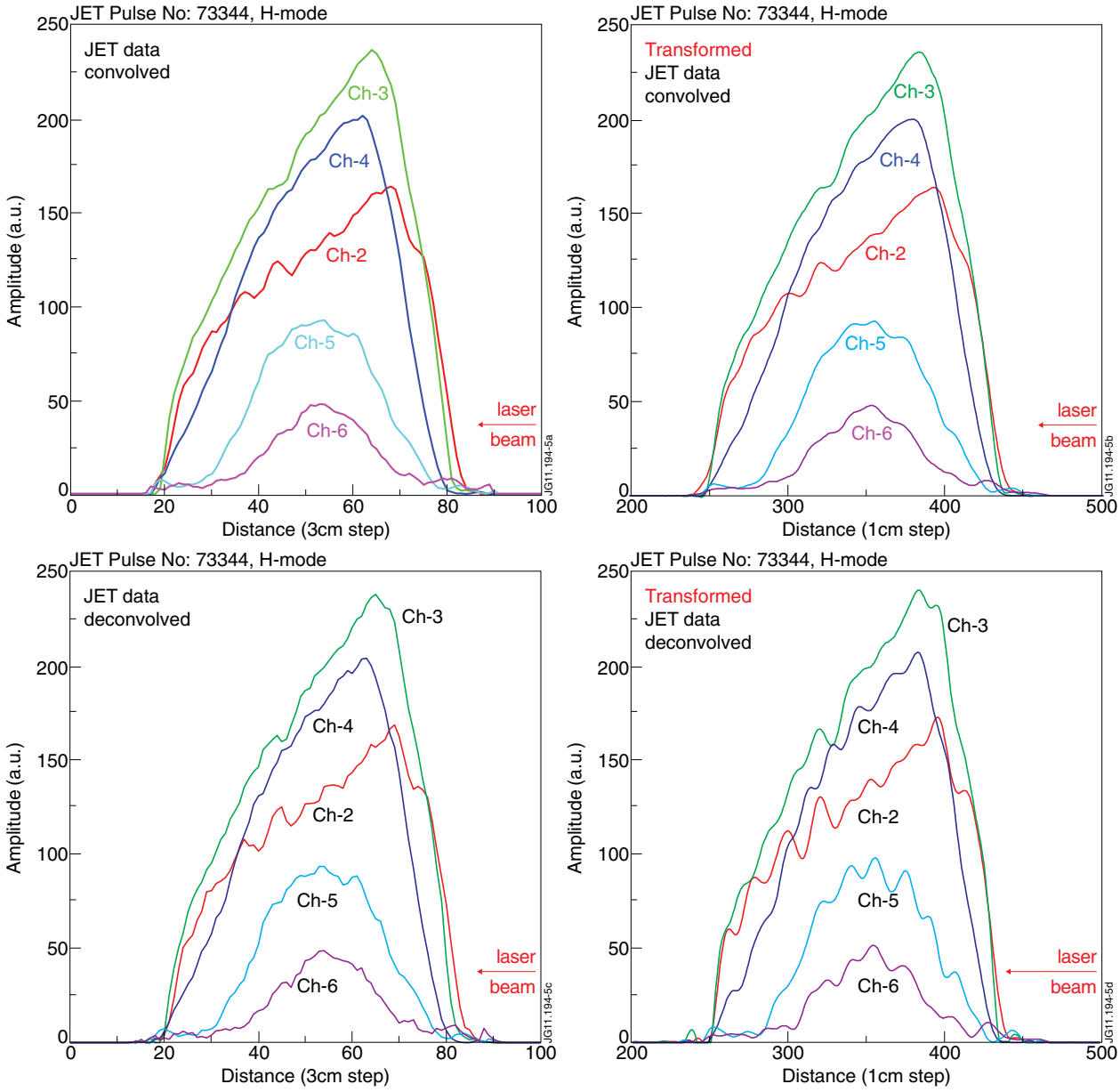

Figure 5: Original convolved (a) and deconvolved (c) LIDAR profiles sampled with a step of 3cm, as well as the corresponding transformed convolved (b) and deconvolved (d) profiles sampled with a step of 1cm.

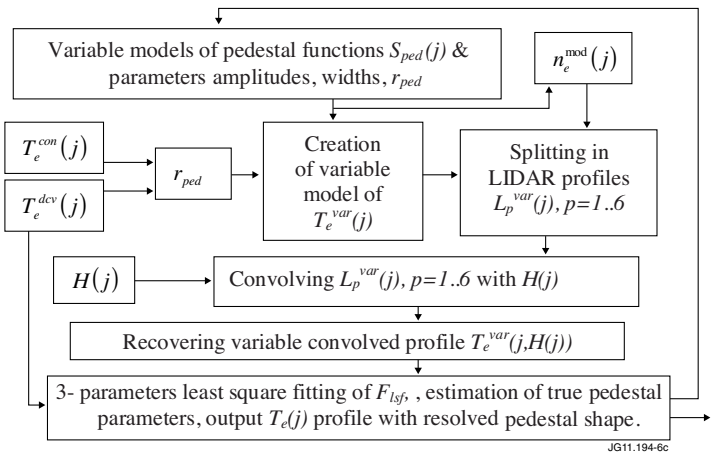

Figure 6: Detailed block-schematic of the algorithm for optimal estimation of the true electron temperature pedestal.

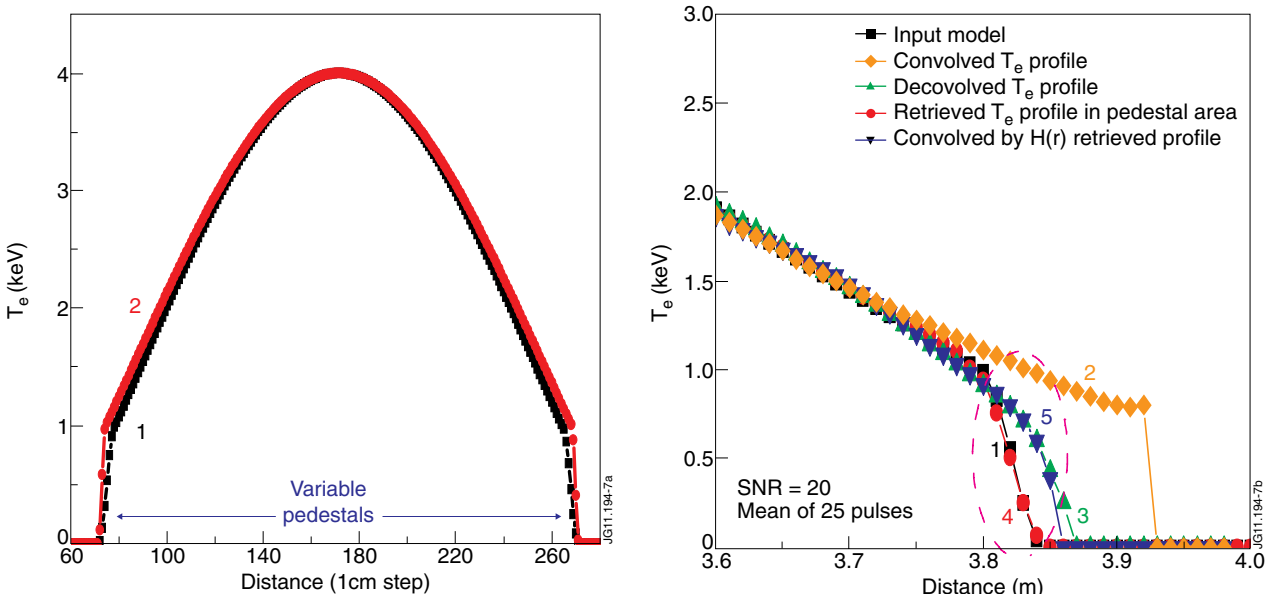

Figure 7. (a) Examples of input electron temperature profiles of variable pedestal parameters. (b) Fitting performance of the optimal algorithm.

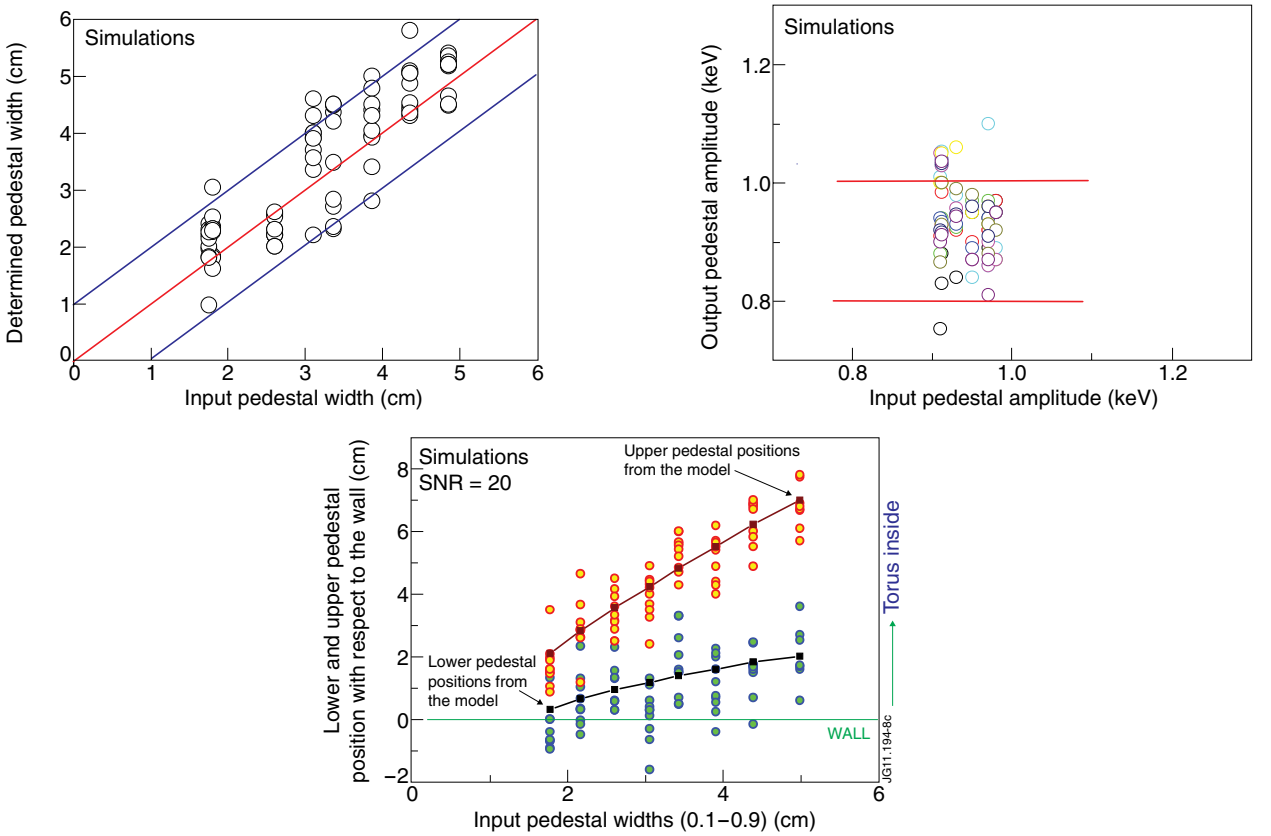

Figure 8: (a) Variations of the retrieved pedestal widths at given input pedestal widths, obtained from a defined set of simulations at SNR = 20; (b) Variations of the retrieved pedestal amplitudes at given input pedestal amplitudes, obtained from a defined set of simulations at SNR = 20; (c) Variations of the upper and lower pedestal positions of retrieved profiles with respect to the corresponding true pedestal positions of the input profiles.

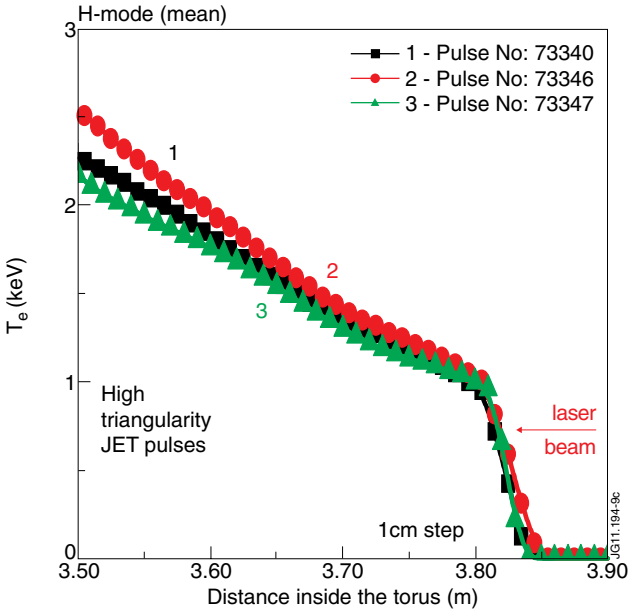

Figure 9: Estimates of true electron temperature pedestal profiles sampled with a step 1cm, retrieved from the mean LIDAR profiles over the H-mode, according to the algorithm described in Sec.4. The JET pulses processed - Pulse No's: 73340 (curve 1), 73346 (curve 2), and 73347(curve 3), are of high triangularity type. The input pedestal shape is of cosine-type.

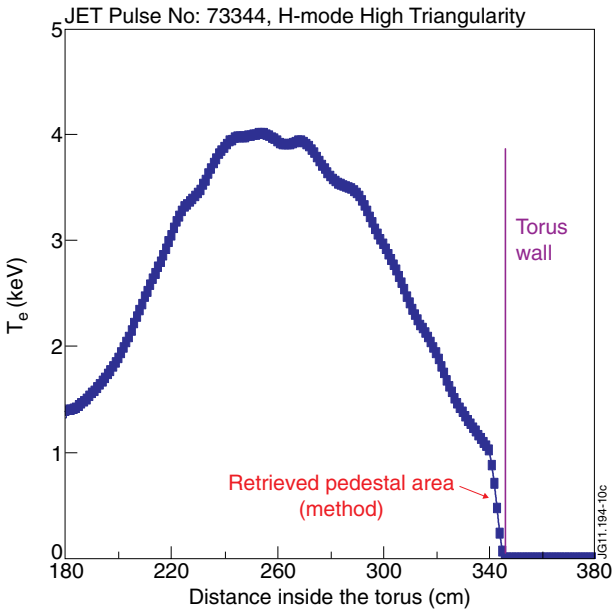

Figure 10: Retrieving of the total electron temperature profile, containing both the resolved pedestal and the profile inside the torus sampled with a finer step of 1cm.